

Testing the application of time-dependent convection in MESA simulations of massive stars

George Abraham

13th September 2024

Abstract

This report focuses on the treatment of time-dependent convection (TDC) in version r24.03.1 of MESA. $20M_{\odot}$ models were run to find any common differences between the treatment of Cox's mixing length theory (MLT) compared to TDC, to thereby ascertain whether using TDC produces more physically accurate results.

Parameters were updated in groups, allowing separation of effects caused by the mixing theory from those of resolution and metallicity, models run on the Lupus server at Keele University and data plotted using Python packages such as mesaPlot.

It was found that changes in mixing theory likely explained differences in central convective velocity treatment and smoothness of convective velocities after an expansion at ~ 10 yr before core collapse. Other effects, including the expansion itself, surface oscillations, He-entrainment during Si-burning and differences in surface and core parameters can be explained by other means (namely metallicity and model resolution).

Qualitatively, it appears TDC and MLT in MESA produce broadly similar results. However, further investigation, changing few parameters at a time and comparing TDC treatment in MESA to 3D models, is needed to show whether this treatment gives results closer to reality.

1 Introduction

This report aims to test the version of Models for Evolution in Stellar Astrophysics, MESA, r24.03.1, focusing on how time-dependent convection (TDC) and Cox's mixing length theory (MLT), referred to in figures as "Cox", affect the behaviour of simulations. To this end, it aims to indicated whether the evolution of a $20M_{\odot}$ star modelled using TDC provides reliable results when compared to MLT.

This is motivated by how a drawback of MLT is its assumption that evolutionary timescales are much longer than convective timescales, making the assumption that convective flux can be time averaged valid. This is, however, not a true assumption for late phases of evolution in massive stars, making time-independence and inappropriate assumption.

Therefore, if an approximation to TDC in 1D, using in the new MESA version provides reliable results (similar to MLT at long timescales, when the above assumption is true), this would indicate modelling with TDC could provide results closer to reality.

2 Theoretical Background

2.1 Advanced Evolution of Massive Stars

After evolution to the main sequence, massive stars of initial mass $M_i \gtrsim 8M_{\odot}$ build a C-O core of mass $M_{\text{core}} \gtrsim 1.06M_{\odot}$ via He-burning to begin ^{12}C -burning, producing isotopes such as ^{20}Ne and ^{24}Mg .

This moves to burning in a shell as Ne-burning begins in a convective core, forming ^{16}O via photo-disintegration and alpha-

capture (for stars $M_i \gtrsim 11M_\odot$). Likewise, this then moves into a shell before O-burning takes place via the $^{16}\text{O} + ^{16}\text{O}$ reaction to form ^{28}Si and ^{32}S within a convective core.

Si-burning begins soon after O-burning moves to a shell, tending towards a final core composition of ^{56}Fe and ^{52}Cr , forming a core primarily of ^{56}Fe before core collapse.

As time progresses, evolutionary timescales become shorter, from $\sim 10^3$ yr for ^{12}C -burning to ~ 1 yr for ^{16}O -burning and only $\sim 10^{-2}$ yr for ^{28}Si -burning, sped up by neutrino emission increasing the rate of core contraction, thereby increasing temperatures between burns. This is reflected in both the ratio of energy generation to energy radiation (via neutrinos; η) and the increase in central density (ρ_c) per unit core temperature (T_c) over time.

Notably, this relation deviates from almost constant proportionality before He-burning, to one with patterns characteristic of each burning stage, deviating from the trend due to the interplay between neutrino loss and temperature increase (Pols, 2011; see Figure 1).

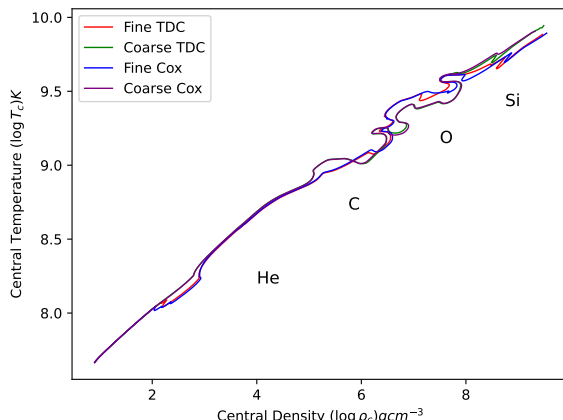


Figure 1: Graph of central temperature (T_c) against central density (ρ_c), plotted from 35% H in the core for four models varying by timestepping and mixing theory. Locations of burning stages are labelled (label locations based on Maeder, 2009).

Kippenhahn diagrams, such as in Figure 2 further aid analysis, showing the evolution of convective burning shells in terms of size (e.g. radius), convection (e.g. Mach number) and time to evolve.

Importantly, because the time between the onset of C-burning and core collapse is shorter

than the dynamical timescale, τ_{dyn} , there is insufficient time for effects experienced at or near the core (such as expansions) to have surface expressions (through changes in luminosity, L , or radius). Hertzsprung Russell diagrams (HRDs), such as in Figure 3, exemplify this, with the majority of change in L and surface temperature, T_{eff} , occurring before C-burning commences.

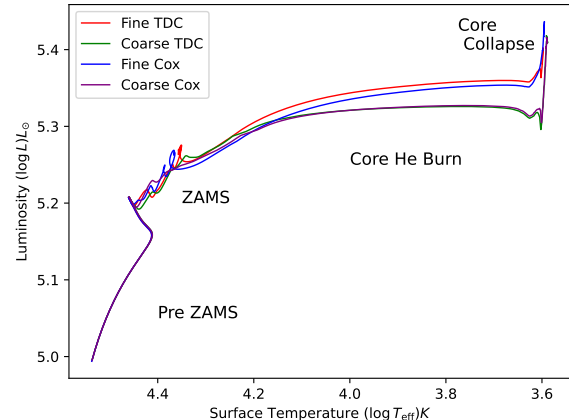


Figure 3: HRD showing change in luminosity by surface temperature of four models from H-burning at 35% core He, varying only by mixing theory and resolution (Fine = high resolution, Coarse = test run resolution). Important stages are labelled (where ZAMS = zero age main sequence; label location after Maeder, 2009).

2.2 Mixing Length Theory

MLT approximates convection within eddies (convective elements) by describing this non-local process by a set of local variables, namely opacity (κ), density (ρ), acceleration due to gravity (g), pressure (P), temperature (T), specific heat at constant pressure (c_p) and energy generation rate, to name a few. These are averaged over the mixing length, l , assumed to be of order pressure scale height, H_P (Weiss et al., 2004).

From these values, it aims to determine a set of temperature gradients (with respect to pressure) to calculate whether a region is convectively unstable. These include the gradient of the surroundings, ∇ , that of an eddy, ∇' and that of matter moving adiabatically, ∇_{ad} . These are coupled with ∇_r , the aver-

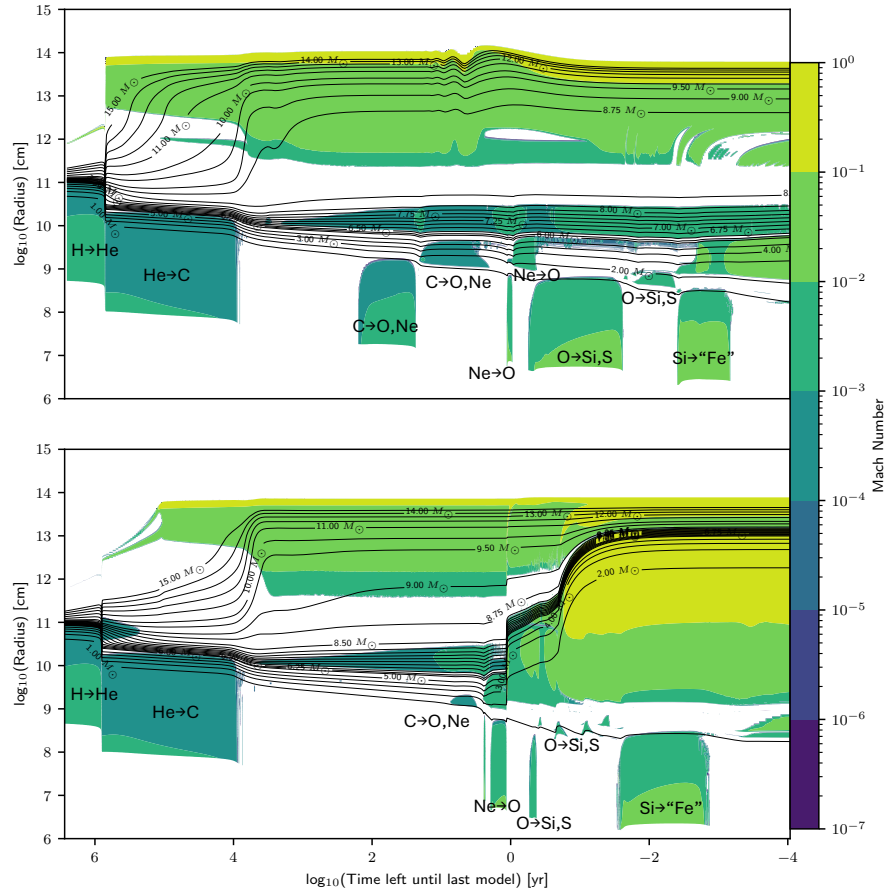


Figure 2: Kippenhahn diagrams of radius (logarithmic) by time until core collapse, comparing a [low metallicity](#) (lower) and [solar metallicity](#) (upper) run using [MLT](#) and short timestepping. Colour pertains to Mach number and label locations are based off of [Pols, 2011](#).

age temperature gradient needed for movement of energy via radiation (with convection suppressed) and ∇_μ , the gradient of molecular weight within an eddy. ([Weiss et al., 2004](#); [Anders & Pedersen, 2023](#)).

To do so, [MLT](#) uses a number of assumptions, namely that hydrostatic equilibrium is maintained (ensuring $\tau_{\text{dyn}} > \tau_e$, the eddy lifetime), turbulent pressure is neglected, convective velocities, \bar{v} , are kept below the local sound speed, v_s and pressure equilibrium is maintained (the anelastic approximation).

This theory combines to give a value for convective efficiency, Γ , indicating whether a point is radiative ($\Gamma \rightarrow 0$) or convective ($\Gamma \rightarrow \infty$) through using the equation

$$\frac{\Gamma}{1-\eta} = \frac{\nabla - \nabla'}{\nabla' - \nabla_{\text{ad}}}. \quad (1)$$

Determining whether an element is convectively unstable is then determined using either

the Leudox criterion,

$$\nabla < \nabla' + \frac{\phi}{\delta} \nabla_\mu, \quad (2)$$

where $\phi/\delta = 1$ if the gas is ideal (as approximately true in a plasma) or the Schwarzschild criterion (used throughout this report),

$$\nabla < \nabla'. \quad (3)$$

The Ledoux criterion accounts for chemical inhomogeneity within a star, whilst the Schwarzschild criterion assumes the star to be chemically homogeneous ([Weiss et al., 2004](#); [von Steinkirch, 2012](#); [Jermyn et al., 2023](#)).

Using theory described, a way of expressing \bar{v} in terms of calculable variables can be derived, leading to the equation

$$\bar{v}^2 = g \nabla_{\text{ad}} \frac{c_P \rho T}{P} (\nabla - \nabla') \frac{l^2}{8 H_P}, \quad (4)$$

where it can be assumed $\nabla' \sim \nabla_{\text{ad}}$ ([Maeder, 2009](#)).

2.3 Time Dependent Convection

[MLT](#) does have pitfalls though, namely that when $\tau_e \geq \tau_{\text{nuclear}}$, the nuclear timescale (as during and after O-burning) accuracy reduces. Also, it doesn't accurately model overshooting or undershooting of convective layers, nor is the growth and decay of convection accounted for.

To improve, time-dependence is added in the form of approximations using fluid equations, namely the Euler equation. Here, we assume free convection, where matter is incompressible (invalid for $\bar{v} \rightarrow v_s$).

However, this is a 3D problem and therefore many assumptions are needed to model this in 1D, namely that $\bar{v} \ll v_s$, microscopic viscosity is neglected and temperature fluctuations are coupled with turbulent velocity (requiring timescales for convection, $\tau > \tau_{\text{dyn}}$; [Weiss et al., 2004](#)).

These assumptions lead to the equation for convective velocity

$$\bar{v}^2 = \frac{1}{6\xi_2^2} \left(J \tan l \frac{H_P + \delta t J}{4} + \xi_1 \right)^2, \quad (5)$$

where

$$J^2 = \xi_1^2 - 4\xi_0\xi_2, \quad (6)$$

$$\xi_0 = \frac{\alpha}{l\sqrt{6}} c_p T \nabla_{\text{ad}} (\nabla - \nabla_{\text{ad}}), \quad (7)$$

$$\xi_1 = \frac{4\sigma T^3}{\rho^2 c_p \kappa} \left(\frac{2\alpha_r \sqrt{3}}{\alpha l} \right)^2 + \frac{2}{3} \alpha_{P_t} \rho \frac{d\rho^{-1}}{dt}, \quad (8)$$

and

$$\xi_2 = - \left(\frac{8}{3} \sqrt{\frac{2}{3}} \right) \frac{\alpha_D}{\alpha l}. \quad (9)$$

Note here that, to ensure convection occurs, it is assumed that $J > 0$ and $J^2 > 0$, whilst the convective flux parameters are usually treated using the default values: $\alpha_r = 0$, $\alpha = 2$, $\alpha_D = 1$ and $\alpha_{P_t} = 0$. Also note that σ is the Stefan-Boltzmann constant and δt is a timestep ([Jermyn et al., 2023](#)).

In MESA r24.03.1, [Jermyn et al. \(2023\)](#) approximates this approach, calculating those solutions of physical interest from solutions to the stellar equations using [TDC](#) theory, whilst

letting the solutions tend to those of [MLT](#) at long timescales (as the theory predicts).

Some physical effects are difficult to recreate in 1D, such oscillations during the (super-) asymptotic giant branch. Here, the instability caused by thermal pulses as a result of an He-shell flash is poorly constrained, meaning convection and mass-loss are poorly understood, thereby making the 1D model difficult to converge ([Rees & Izzard, 2024](#)).

3 Data

Simulations were run on the LUPUS server at Keele University, all based upon the original test suite `20M_pre_MS_to_core-collapse` provided by version r24.03.1 of MESA.

35 simulations were run from 21st June to 2nd August using up to 6 cores on the server.

4 Method

For each simulation, inlist parameters were edited using the [Fortran](#) language, updating the default test suite values to emulate those used by [Whitehead \(2024; priv. comm.\)](#) in version r10398. Here, difficulties were found with the difference in syntax between the two versions and how the test suite used here utilises multiple inlists (changing parameters at different stellar evolutionary stages).

Throughout, the approach was to update parameters and find the effect of this using [MLT](#) and [TDC](#) (comparing the outcomes). Parameters were grouped into the categories: mixing, metallicity, timestepping and miscellaneous parameters, edited in these groups from the default to either that used by [Whitehead](#) or the recommended value for a production run within the test suite (if the parameter did not exist in version r10398).

This method, whilst enabling analysis of a range of observable effects would, however, have benefited from changing only a few parameters at a time to increase confidence as to their causes (not possible here due to time constraints).

Meanwhile, a number of values remained constant, notably including the mass ($20M_\odot$)

and convection theorem (Schwarzchild; see Section 2.2).

4.1 Data Analysis

To analyse the simulations, profiles (taken every 10 models, storing detailed location-dependent data) and history files (providing more generalised information for each model) were processed using a number of Python libraries, namely `mesaPlot` (for plotting isotopic abundances and Kippenhahn diagrams), `mesa_reader` (for reading profile and history files) and `mesa_EDDY` (to plot more detailed Kippenhahn diagrams).

Plotting isotopic abundances over mass at different points allowed analysis of shell mergers (affected by the style of convection) whilst **HRDs** gave an understanding of effects experienced on the stellar surface and graphs of T_c by ρ_c showed those at the core (see Section 2.1).

4.2 Limitations

Due to the nature of 1D stellar models, it is often difficult to discern whether an observed effect has physical meaning, is numerical, or a mixture of both. Therefore, a range of other parameters were plotted, such as surface radius over time and temperature over radius, to thereby aid in understanding results at different points during a model.

This is also the stimulus for running models with small parameter changes, providing an indication of whether the cause of an effect is the change in a physical parameter (e.g. metallicity) or something numerical (e.g. timestepping).

5 Results and Discussion

After analysis, a number of interesting effects were found. Some were expressed differently between **MLT** and **TDC** whilst others presented in both, requiring further investigation to ascertain whether the cause.

5.1 Overall Comparison

Firstly, to understand the general impact of changing the mixing theory, the surface and

core conditions were investigated.

Figure 1 shows how the core conditions (the relation between ρ_c and T_c) are similar between all models shown for the early evolution, only diverging after C-burning, though even at this point by qualitatively small degrees. The greatest change in style of burn is, in fact, seen when the timestepping is changed.

Likewise, Figure 3 shows a similar story, where all models show consistent L by T_{eff} relationships up to **zero-age main sequence (ZAMS)**. Notably, however, the greater resolution led to increased differences between **MLT** and **TDC** after this point.

The similarities seen in the **HRD** before core collapse were likely a result of how the envelope and core were decoupled at this point (see Section 2.1).

5.2 Central Velocity

Throughout, though most obvious during H-burning, Mach number (M) and \bar{v} modelled using **MLT** increases steeply toward the centre, whilst those modelled using **TDC** and those calculated using Equation 4 (for both **MLT** and **TDC**) tend to zero (see Figure 4a).

This is surprising, since at such an early stage it is expected that, since timescales are long, **MESA** will approximate **TDC** as **MLT**, meaning both values given for M and \bar{v} would be equal (see Section 2.3).

This effect is likely caused by the differing treatment of conditions at the core: a difficult location to model in a 1D scenario.

Notably, in a 3D model from [Georgy et al. \(2024\)](#) \bar{v} values during Ne-burning appear to increase toward the core (as implied by modelled **MLT** values), though the overall profile shape should increase from a low, as predicted by **TDC** and **MLT** calculated with Equation 4.

The difference in treatment between values of \bar{v} and M calculated and given by **MESA** is further highlighted in Figure 4b. Here, values calculated by **MESA** appear to be a factor larger than those found using Equation 4 for both mixing theories.

This finding indicates Equation 4 doesn't treat the envelope in the same way as by **MESA**, whilst showing envelope convection is treated similarly by both mixing theories.

That said, values for **TDC** and **MLT** calculated by **MESA** are nearly equal in Figure 4b, indicating treatment of \bar{v} is still similar, even at short timescales.

5.3 Helium Entrainment

In most models run, during Si-burning a number of shells are merged, creating a new shell which 4He is drawn into over time.

This is illustrated in Figure 5, where ^{40}Ca and ^{28}Si are drawn up whilst ^{20}Ne and ^{24}Mg are drawn to deeper regions at $\log_{10}(\text{time to core collapse}) \sim -3.1$. The similar outcome of models using different mixing theories suggests the change does not qualitatively effect the outcome of this event, even given the short timescales for burning at this point.

5.4 Shell Merger $\sim 1\text{yr}$ to Core Collapse

Approximately one year before core collapse, the majority of models run at **low metallicity** (using either mixing theory) showed a large shell merger, leading to an expansion. Notably though, the isotopes involved in the merger differed slightly between models (some occurring during O-burning, whilst others during or toward the end of C-burning).

Comparing Figures 2 (the lower diagram) and 6 also show how the merger style varies, with 2 expanding in two stages (at the end of Ne-burning and then when O-burning moves to a shell).

Such a difference may, however, be numerical, since the models are equal in mixing theory, metallicity and resolution, meaning further investigation is needed to find the cause.

Figure 6 shows that, at the point of expansion, using **MLT** leads to the creation of radiative pockets, whilst using **TDC** leads to a more homogeneous convecting envelope. The timing of the expansion also differs, beginning earlier when using **MLT** than with **TDC**.

The former effect could suggest that **TDC** provides a more realistic representation of envelope convection than **MLT**.

The cause may be a smoothing effect created when treating **TDC** in 1D, since fluid

variables, 3D and local in nature, are approximated to 1D using averages (see Section 2.3).

The latter observation, meanwhile, is expected, since the short timescale and large uncertainty inevitably leads to timing inconsistencies between models during the late stages of evolution.

5.5 Surface Oscillations

Oscillations in surface radius at $\sim 10\text{yr}$ to core collapse were also observed, increasing in amplitude before dying away. Notably, they only feature in high resolution models, where low resolution models show more erratic changes in radius (see Figure 7).

The magnitude of such oscillations do, however, vary dramatically. Figure 2 shows how the **solar metallicity** model clearly shows this oscillatory pattern, expressed throughout the envelope, whilst the **low metallicity** model expresses this at scales too small for the diagram.

The cause is likely numerical, owing to how surface oscillations are expected during phases of instability, such as during the red supergiant phase, but they were not possible to accurately recreate with the model used (see Section 2.3).

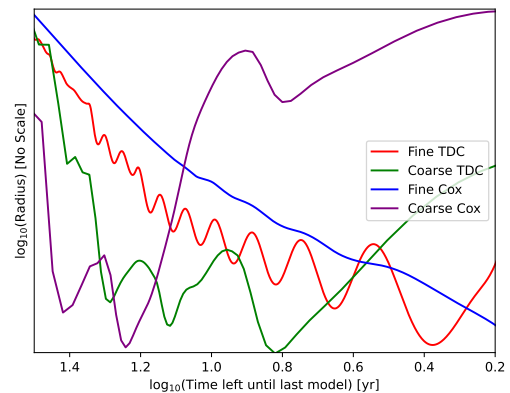
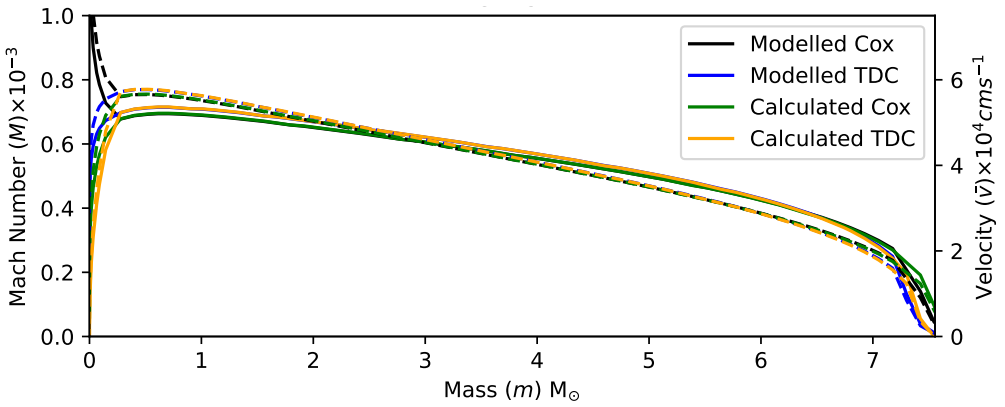


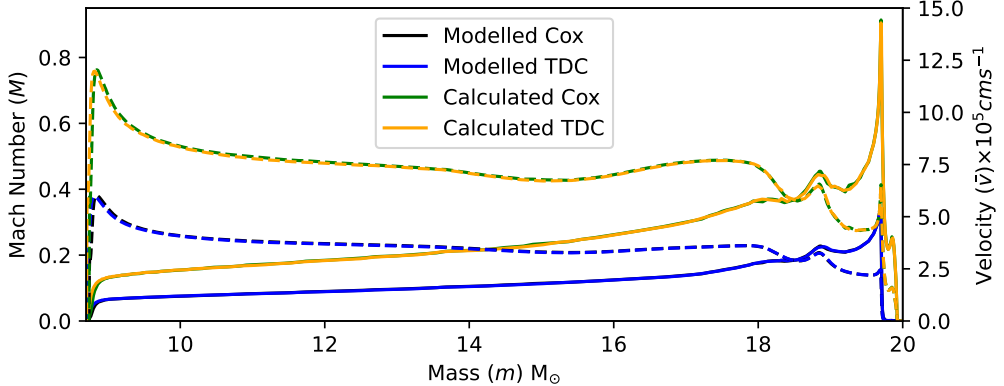
Figure 7: Relative change in stellar radius in four models, varying only by mixing theory and resolution (Fine = high resolution, Coarse = test run resolution).

6 Conclusion

This report aimed to determine whether the new treatment of convection using **TDC** by **MESA** is more physically accurate compared to **MLT**.



(a) Convection shown is in the core region at 35% core H to burn ($\log(\text{time to core collapse})$ is $\sim 6.41\text{yr}$ for both models).



(b) Convection in the envelope during O burn, close to core collapse. ($\log(\text{time to core collapse})$ is $\sim -0.35\text{yr}$ for **MLT** and $\sim -0.38\text{yr}$ for **TDC**).

Figure 4: Graphs of Mach number and convective velocity by mass location. *Modelled* pertains to the use of Equation 4 and *Calculated* to that directly calculated by **MESA**. Dashed lines are convective velocity measurements and full are Mach number.

Using the Luples server at Keele University, models were successfully run comparing outcomes using these to theories and, after analysis, a number of interesting effects were noticed.

Convective velocities at the centre were found to be constrained differently when using **MLT** compared to **TDC** and velocities calculated from gradient variables.

Shell mergers were also observed, though those involving He-entertainment varied little between mixing theories, whilst those occurring at $\sim 1\text{yr}$ to core collapse depended primarily on metallicity, save for the introduction of radiative zones in the envelope with **MLT** when the expansion caused by the merger occurred, differing from the more homogeneous envelope when using **TDC**.

Some oscillatory effects were also observed in some models, though this was thought to be

mainly a numerical result, only observed when models were well-resolved.

Overall, deviation between the outcome of **MLT** and **TDC** is small compared to effects from changes in resolution (significantly altering the core and surface conditions) and metallicity.

That said, those differences observed have the potential to alter the outcome of evolution both during early and late stages, therefore warranting further investigation to ascertain whether the use of **TDC** by **MESA** is more physically accurate overall, thereby indicating whether it should be the preferred option for future 1D models.

The methodology used should, however, be improved. Updating only a few parameters every model would provide greater confidence to the cause of observed effects, providing more confidence to future findings.

In future, **MESA TDC** models should be

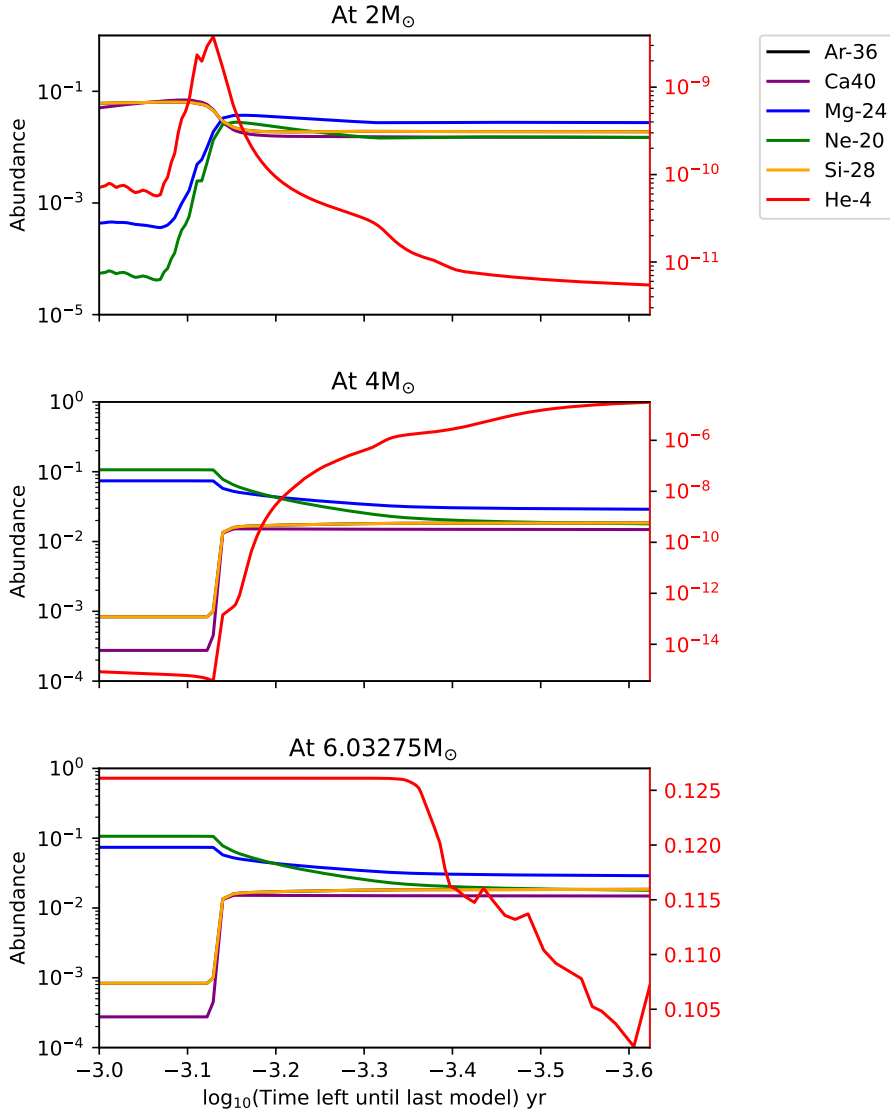


Figure 5: Isotopic abundances over time during the He shell merger event in a high resolution time-dependent convection run for three locations ($2M_{\odot}$, $4M_{\odot}$, $6.03275M_{\odot}$), where the right axis relates to He-4 abundance.

compared to 3D models at late evolutionary stages, known to accurately model true TDC, thereby indicating whether the 1D approximation is a realistic one.

Acknowledgements. I am grateful to the School of Chemical and Physical Sciences at Keele University for providing me with the opportunity to work in a research group and for the support they provided through a bursary. I also thank Raphael Hirschi for supervising me and providing a lot of guidance and support along the way, Vishnu Varma for greatly helping me to understand the literature and results whilst giving many suggestions of how to develop the project and Emily “Em” Whitehead for her help with coding and understanding the data. Lastly, I am thankful

to all the physics post graduate researchers at Keele University for being so welcoming and for providing so much helpful advice along the way.

References

- Anders, E. H. & Pedersen, M. G. 2023, Galaxies, 11, 56
- Georgy, C., Rizzuti, F., Hirschi, R., et al. 2024, Monthly Notices of the Royal Astronomical Society, 531, 4293
- Jermyn, A. S., Bauer, E. B., Schwab, J., et al. 2023, The Astrophysical Journal Supplement Series, 265, 15

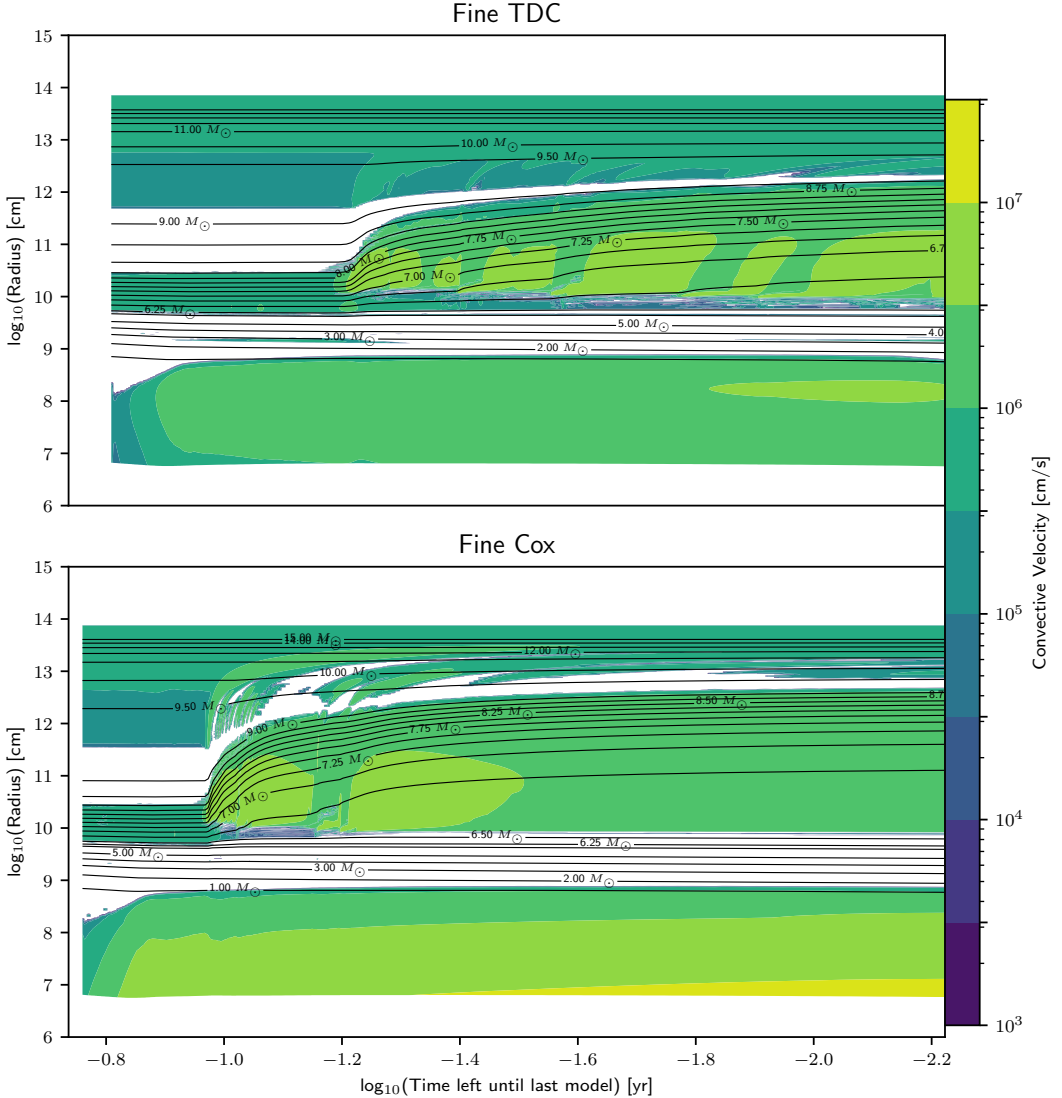


Figure 6: Kippenhahn diagrams of radius (logarithmic) by time until core collapse, comparing an **MLT** (lower) and **TDC** (upper) run using short timestepping, focusing on a shell merger. Colour pertains to convective velocity.

Maeder, A. 2009, Physics, Formation and Evolution of Rotating Stars, 1st edn., Astronomy and Astrophysics Library (Berlin, Heidelberg: Springer-Verlag)

Pols, O. 2011, Stellar Structure and Evolution, Lecture Notes (Utrecht University), 175–186

Rees, N. R. & Izzard, R. G. 2024, Monthly Notices of the Royal Astronomical Society, 531, 4033

von Steinkirch, M. 2012, The Ledoux Criterion for Convection in a Star, Lecture Notes (State University of New York at Stony Brook), 5–7

Weiss, A., Hillebrandt, W., Thomas, H.-C., & Ritter, H. 2004, Cox & Giuli's Principles of Stellar Structure, 2nd edn. (Cambridge: Cambridge Scientific Publishers Ltd)

Whitehead, E. 2024, personal communication

Appendices

A Glossary

Terms

low metallicity Defined here as initial hydrogen mass fraction of 0.001 and initial helium

mass fraction of 0.2496571429.. [3](#), [6](#)

solar metallicity Defined here as initial hydrogen mass fraction of 0.0142 and initial helium mass fraction of 0.2703.. [3](#), [6](#)

Acronyms

HRD Hertzsprung Russell diagram. [2](#), [5](#)

MLT Cox's mixing length theory. [1](#)–[7](#), [9](#)

TDC time-dependent convection. [1](#), [4](#)–[9](#)

ZAMS zero-age main sequence. [5](#)

Symbols

H_P Pressure scale height. [2](#)–[4](#)

L Luminosity. [2](#), [5](#)

M_{core} Stellar core mass. [1](#)

M_i Initial mass of star. [1](#), [2](#)

M Mach number. [5](#)

P Pressure. [2](#), [3](#)

T_c Central temperature. [2](#), [5](#)

T_{eff} Effective temperature. [2](#), [5](#)

T Temperature. [2](#)–[4](#)

Γ Convective efficiency. [3](#)

α_D Convective flux parameter, set to 0 by default. [4](#)

α_{P_t} Convective flux parameter, set to 0 by default. [4](#)

α_r Convective flux parameter, set to 0 by default. [4](#)

α Convective flux parameter, set to 2 by default. [4](#)

\bar{v} Average convective velocity. [3](#)–[6](#)

δt Numerical timestep. [4](#)

η Ratio of energy generation to energy radiation. [2](#), [3](#)

κ Opacity. [2](#), [4](#)

∇' Average temperature gradient with respect to pressure for a convecting element. [2](#), [3](#)

∇_{ad} Average temperature gradient with respect to pressure for matter moving adiabatically. [2](#)–[4](#)

∇_r Average temperature gradient needed for movement of energy via radiation (with convection suppressed). [2](#)

∇_μ Average molecular weight gradient with respect to pressure within an element. [3](#)

∇ Average temperature gradient with respect to pressure for all matter at given level. [2](#)–[4](#)

ρ_c Central density. [2](#), [5](#)

ρ Density. [2](#)–[4](#)

σ Stefan-Boltzmann Constant. [4](#)

τ_{dyn} Dynamical timescale. [2](#)–[4](#)

τ_e Opacity. [3](#), [4](#)

τ_{nuclear} Nuclear timescale. [4](#)

c_P Specific heat at constant pressure. [2](#)–[4](#)

g Local acceleration due to gravity. [2](#), [3](#)

l Mixing length. [2](#)–[4](#)

t Time. [4](#)

v_s Local speed of sound. [3](#), [4](#)